Transport of intense particle beams in large scale plasmas

B. Chen,[1] D. Wu,[2,*] J. Ren,[1] D. Hoffmann,[1] and Y. Zhao[1,†]

[1] *School of Science, Xi'an Jiaotong University, Xi'an 710049, China*

[2] *Institute for Fusion Theory and Simulation, Department of Physics, Zhejiang University, Hangzhou 310058, China*

(Dated: September 5, 2019)

Transport of particle beams in plasmas is widely employed in fundamental research, industry and medicine. Among such fundamental research and applications, beam-plasma instabilities play a significant role. Due to high inertia of ion beams, their transport in plasmas are usually assumed to be stable. Here we report the formation and development of sausage instability and kink instability, when studying the transport of intense proton beams in large scale plasmas by using a newly developed particle-in-cell simulation code. Simulation and analysis indicate the self-generated magnetic fields, produced by movement of collisional plasmas, are the dominant drivers for such instabilities. When analysing the instability growth rate and energy loss of injected proton beams, sausage instability and kink instability are found to be significantly determined by the injected beam densities and energies. Our finding might find great applications in inertial confinement fusion researches and also might be of interests to the laboratory astrophysical community.

PACS numbers: 52.35.Bj, 52.40.Mj

The transport of particle beams in plasmas is of great research interests in foundamental research and applications, such as accelerator physics [1, 2], high energy density physics [3], inertial confinement fusion (ICF) [4] as well as astrophysical shocks [5, 6] and cosmic rays [7, 8] in space and astrophysical plasmas. Beam-plasma instabilities play an important role, because of their great varieties [9, 10] and also because they significantly influence the distribution and dynamics of the beams. For specific applications, they certainly should be controlled, for example, the fast ignition inertial confinement fusion [11] and plasma wakefield acceleration [12, 13]. While for some fundamental astrophysical research, instabilities by themself are the essential research efforts. For example, with the formation of astrophysical collisionless shocks and energetic cosmic rays, supersonic flows generate electromagnetic fields through instabilities and particles can then be accelerated to high energy cosmic rays [14–17].

As simulations of inertial confinement fusion or plasma astrophysics are usually large in spacial and temporal scales, for a long time, fluid approaches [18–22] have dominated the research. Since fluid approaches can not include micro-kinetic processes, like acceleration or deceleration of particles and kinetic instabilities, in recent years, there was pressure to change the view of plasmas from fluid to kinetic methods. Particle-in-cell (PIC) simulation method [23–27] has established itself as a state of the art method in kinetic plasma physics. It is a compromise between direct particle interaction, i.e. molecular dynamics [28–30] or N-body method [31–33], and Vlasov methods [34–36]. It has proven to be a valuable tool in understanding many astrophysical phenomena from first principles [37, 38].

PIC method is able to provide a great variety of information of complex and dynamic systems. However, when the densities of particle beams and plasmas differ by orders of magnitude, e.g., the beam density is three orders smaller than plasma density [39], direct PIC simulation of beam-plasma interaction becomes very challenging. This is because, when spacial and temporal scales are normalized by low density particle beams, simulation of high density plasma leads to significant numerical self-heating and instabilities; when normalized by high density plasmas, simulation demands dramatically huge simulation grids and time steps, which is currently an unaffordable task for state-of-art super-computers. However, the in-

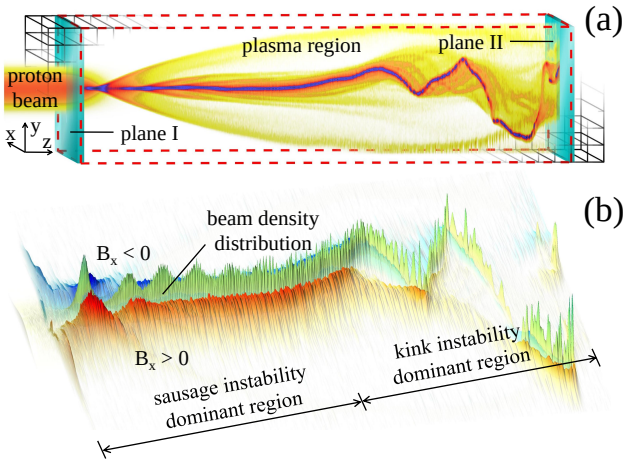

FIG. 1. (a) Schematic representation of the simulation model. Plasma is uniformly distributed within the red dashed box initially. Plane I and II are two positions where the beam energy is measured. The black cuboids present the cells in the simulation. (b) Beam transport with the self-generated magnetic constraint. The red and blue surfaces stand for the self-generated magnetic fields in x direction which are respectively positive and negative. The green surface between them is the proton beam density distribution.

* dwu.phys@zju.edu.cn

† zhaoyongtao@xjtu.edu.cn

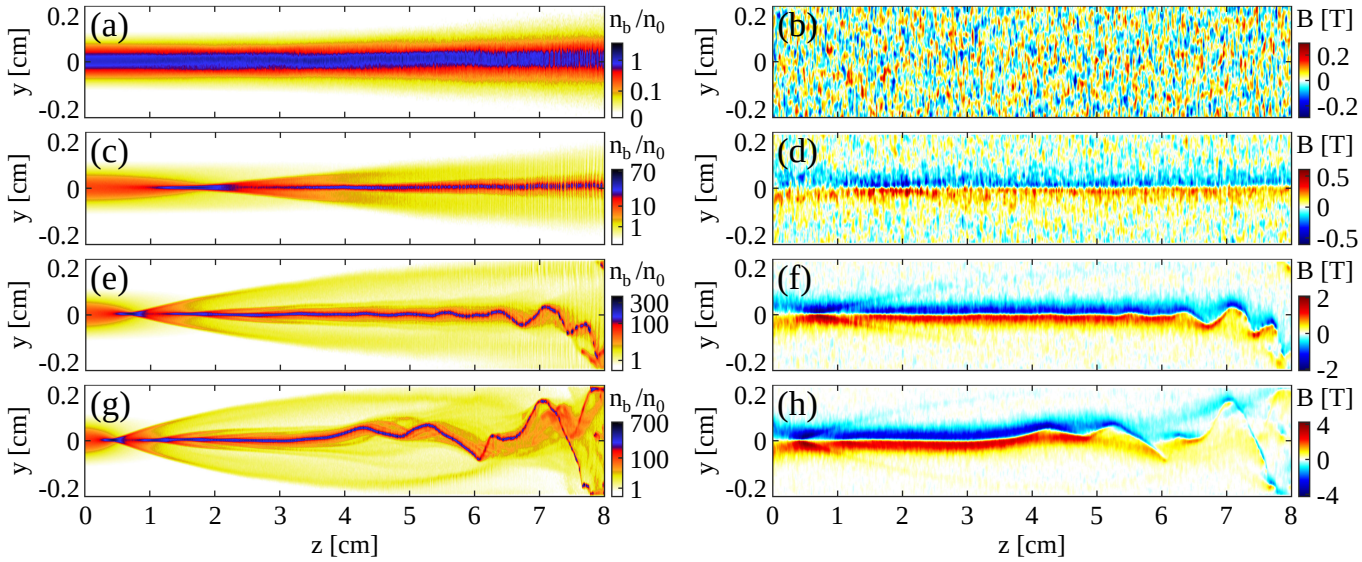

FIG. 2. The distributions of beam densities and magnetic fields for proton beams with different densities at $t = 12$ ns. (a), (c), (e) and (g) stand for the proton beam density (in unit of $n_0 = 10^{14}$ cm^{-3}), with initial densities of 1×10^{14}, 1×10^{15}, 5×10^{15} and 1×10^{16} cm^{-3} and injection energies of 0.4 MeV, respectively. Note, the corresponding current densities are 1.4×10^{8}, 1.4×10^{9}, 7×10^{9} and 1.4×10^{10} A/m^2. (b), (d), (f) and (h) are connected magnetic fields.

teractions with large density difference widely exists in astrophysical plasmas [5–8] and inertial confinement fusion [4] researches. For example, in fast ignition inertial confinement fusion [40], intense electron beams are produced by picosecond relativistic laser beams and then injected into high density plasma. Here, the density of intense electron beam is of 10^{21} cm^{-3} and plasma density is of 10^{25} cm^{-3}. Therefore a kinetic method that can simulate plasmas with large density difference or with large spacial and temporal scales is of great importance and emergency. In a recent work, an advanced numerical method that combines the PIC method with a reduced model of high density plasma based on Ohm's law was proposed [41] and benchmarked. With this method, it is now possible to reveal the untouched phenomena in large scale beam-plasma interactions with density differences by orders.

Here, the transport of continuous proton beams in plasmas with density of 10^{18} cm^{-3} and size of 8 cm is simulated by LAPINS PIC code [41–45] for more than 10 nano-second (ns). In the simulations, densities of injected proton beam vary from 10^{14} cm^{-3} to 10^{16} cm^{-3} and the energies of injected protons range from 0.4 MeV to 4.0 MeV. We here take such a simulation setup by considering the following two reasons. Firstly, plasma gas cell and continuous proton beams with similar densities, sizes and energies are nowadays well available. Therefore, in principle, the simulation predictions can be confirmed by experiments. Secondly, according to the theory of similarity [46], where the key role is played by dimensionless parameters that characterize the phenomena under consideration, such simulations might also be of relevance for astrophysics and fast ignition inertial confinement fusion.

The system setup is displayed in Fig. 1(a), here hydrogen plasma of density 10^{18} cm^{-3} and temperature of 4 eV is uniformly distributed with lengths along z of 8 cm and along y of 4 mm (within the red dashed box). A continuous proton beam with a radial Gaussian distribution and a width of 0.8 mm is injected into the plasma along z axis at $t = 0$. For two-dimensional simulations, there are 2250 grids in z direction and 100 grids in y direction. The time step of simulation is 67 fs. Absorbing boundary conditions are imposed on the particles and fields in z direction, while in y directions, periodic boundary conditions are applied instead. Two diagnostic planes marked plane I and plane II are used to measure particle energies. In this Letter, we report the formation and development of sausage and kink instabilities for transport of intense proton beams in large scale plasmas. As shown in Fig. 1(b), such instabilities are found significantly connected to self-generated magnetic fields. Further simulation and analysis indicate such magnetic fields are produced by movement of collisional plasmas. When analysing the instability growth rate and energy loss of injected proton beams, such instabilities are found to be significantly determined by the injected beam densities and energies.

In order to figure out the triggering and evolution of sausage and kink instabilities, we scanned the injected proton beams with fixed energy 0.4 MeV and varying densities from 10^{14} cm^{-3} to 10^{16} cm^{-3}. Figure 2 displays the maps of proton beam density and magnetic fields at $t = 12$ ns. When density of injected beam is 10^{14} cm^{-3} as shown in Fig. 2(a), transport of protons in plasmas is quite ordinary. The beam is straightforward

and only slightly deflected at the front end by collisions with background plasmas. For such a large density difference between injected proton beam and background plasmas, the collective electromagnetic field can hardly be generated. As shown in Fig. 2(b), magnetic field is even smaller than background fluctuations. Further simulations confirm that when the proton beam density is lower than 10^{14} m^{-3}, the collective effect of the plasma on the proton beam is not of significance at all.

When the proton beam density increases to 1×10^{15} and 5×10^{15} cm^{-3}, Fig. 2(c)-(f), show significant beam focusing during the beam transport. Similar beam focusing had been reported in beam driven plasma wakefield acceleration studies [13]. However unlike the ones in plasma wakefields, moving with the beam, here the focusing positions of beam are almost fixed. Moreover, distances between focusing positions are of centimeters. If the plasma wakefield theory still works under such situations, the spacing should be less than one millimeter. When increasing beam densities, the focusing effect is significantly intensified and the distance between focusing positions is shortened. All these phenomena imply a new mechanism of beam focusing effect, which is quite different from wakefield modulations [39]. In Fig. 2(d) and (f), the self-generated magnetic field, as a result of beam current and neutralizing current in collision plasmas, is obviously stronger than background fluctuation.

In the analysis, it is assumed that the proton beam propagates along the z direction, while the radial and angular directions are denoted by r, θ respectively. The initial perturbation is written as $\boldsymbol{\xi}(\boldsymbol{r}) = \boldsymbol{\xi}(r)\exp[i(m\theta + kz)]$, a function of r, θ, z, where parameter m and the angular wave number k_θ satisfy $m/r = k_\theta$, and k is the wave number in z direction. When $m = 0$, the perturbation does not depend on the angular direction, and the stable condition of the proton beam [47] is $-(r/P_0)(\partial P_0/\partial r) < 2\gamma B_\theta^2/(\gamma P_0 + B_\theta^2)$, where P_0 is the pressure, B_θ is the angular magnetic field and γ is the adiabatic index (heat capacity ratio), which is 5/3 in our case. As the proton beam satisfies the radial Gaussian distribution, the larger the coordinate in the radial direction, the smaller the density and the pressure. Therefore, we have $\partial P_0/\partial r < 0$. Assuming an initial perturbation making the proton beam shrink and become thinner radially, the corresponding $|\partial P_0/\partial r|$ will increase. At some point, the left side of the inequality might be larger than the right side. The break of the stability condition results in this sausage instability. Since $m = 0$, this instability is axially symmetric. The magnetic fields in the contraction regions are stronger than those in other regions, which further leads to larger magnetic pressure. As the contraction grows, the beam density in this region increases simultaneously. So do the collision and thermal pressure. The beam transports under the constrain of magnetic field as illustrated in Fig. 1(b). When the magnetic pressure matches the thermal pressure, the instability stops growing and a fixed focus point is then formed at the contraction area. As the initial beam density gets higher from 1×10^{15} cm^{-3} to 5×10^{15} cm^{-3}, the magnetic pressure will grow even faster and, thus, form the focus point earlier at a lower z position, which is consistent with the distribution of the proton beam and magnetic field showed in Fig. 2(c) to (f).

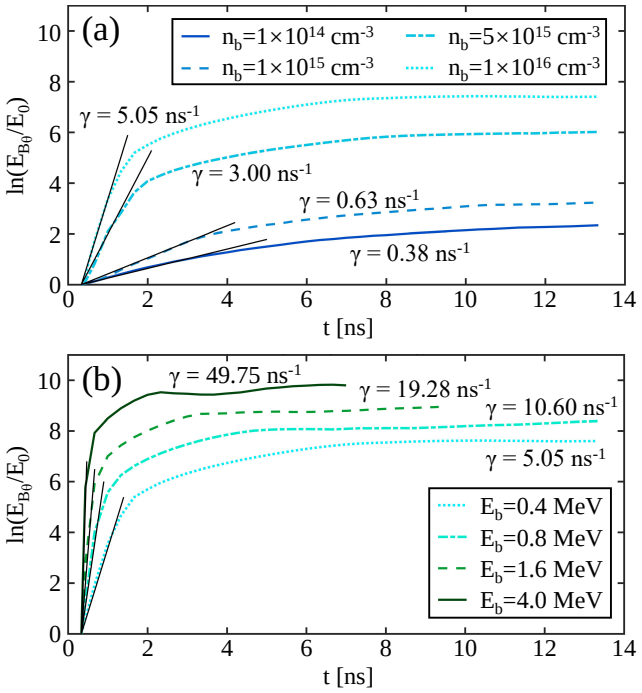

FIG. 3. Time evolution as a function of time: (a) the angular magnetic field energy for proton beams with fixed 0.4 MeV but with different densities, and (b) the angular magnetic field energy for proton beam with fixed density 10^{16} cm^{-3} but with different energies. The slope of the black lines stands for the growth rate in linear stage.

In our simulation, the initial perturbations actually result from the collision and get boosted by the magnetic field. According to Ref. [41], the beam current $\boldsymbol{J}_b$ and magnetic field $\boldsymbol{B}$ are connected by Ohm' law, $\boldsymbol{E} + \boldsymbol{v}_e \times \boldsymbol{B} = \eta \boldsymbol{J}_b$ and Faraday' law $\partial \boldsymbol{B}/\partial t = -\nabla \times \boldsymbol{E}$, where $\boldsymbol{v}_e$ is the background electron velocity, and η is the resistivity. For small electron velocity, we have $\boldsymbol{B} = -\int dt \nabla \times (\eta \boldsymbol{J}_b)$. When the beam density is 10^{14} cm^{-3} in Fig. 2(b), the magnetic field is basically a background noise, which is around 0.2 T. While it can be as large as 2 T when beam density in 5×10^{15} cm^{-3} as shown in Fig. 2(f). The transverse magnetic pressure on proton beam, i.e. the perturbation, will increase by 100 times.

When the proton beam density reaches 5×10^{15} cm^{-3} and 1×10^{16} cm^{-3} as shown in Fig. 2(e) and (g), it is worth noting that the spatial distribution of the proton beam in high z region undergoes another change along with sausage instability. The transport path of the proton beam is no longer a straight line along the axis, but a curved path around it. The same curved features also appears in the magnetic fields as shown in Fig. 2(f) and (h). This is due to another instability – kink instability.

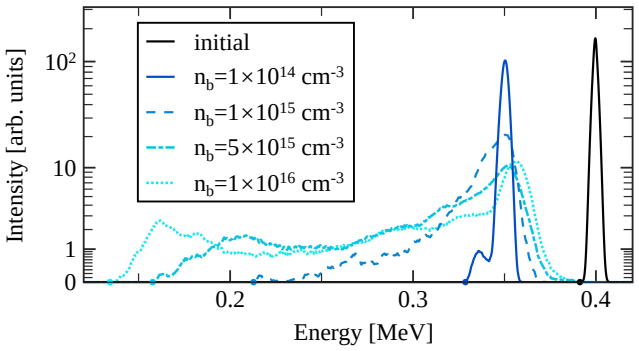

FIG. 4. Beam energy spectra for different densities measured by plane II at $t = 13.33$ ns. The black curve is the initial spectra of these beams, detected by plane I. The dots at the bottom are the minimum energies detected of each case.

TABLE I. Beam density (BD), averaged energy (AE), minimum energy (ME) and energy loss percentage (ELP) after passing through plasmas for four simulation cases with different densities.

Parameters	Case-1	Case-2	Case-3	Case-4
BD, cm^{-3}	1×10^{14}	1×10^{15}	5×10^{15}	1×10^{16}
AE, keV	350	337	307	296
ME, keV	330	215	160	139
ELP	12.5%	15.8%	23.3%	26.0%

Considering the perturbation function, when $m \neq 0$, the perturbation is related to the angular coordinate, and the stability condition of the proton beam [47] is written as $(r^2/B_\theta)(\partial B_\theta/\partial r) < (m^2-4)/2$. The angular magnetic field B_θ is proportional to $1/r$ outside the proton beam. Therefore we have $(r^2/B_\theta)(\partial B_\theta/\partial r) = -2$, which means the stability conditions are satisfied for all $m \neq 0$. Inside the proton beam, B_θ and r are proportional. When $m = 1$, the stability condition will no longer be satisfied. In this case, the kink instability related to the angular coordinate appears. Supposing the proton beam is bended by an initial perturbation, it will become further kinked due to the magnetic pressure difference around the beam. Actually, when the protons arrive at the positions of maximum y values, the outer magnetic fields have to be larger than the inner magnetic fields in order to drive protons back. Such magnetic field distribution is displayed in Fig. 2(f) and (h).

To study the instabilities quantitatively, the growth rate should be evaluated. Here we get the instability growth rate by analysing the angular magnetic field energy, $E_{B_\theta} = \sum B_\theta^2/8\pi\delta x\delta y\delta z$. It can be related to the growth rate when written as $E_{B_\theta} \sim \exp(\gamma t)$, where γ is the growth rate.

The angular magnetic field energies E_{B_θ} and corresponding growth rates γ for fixed 0.4 MeV beams with different densities as functions of time are displayed in Fig. 3(a). The logarithmic energy increases sharply at first in linear stage, and then followed by a non-linear saturation stage. We find the magnetic energy of higher beam density rises faster. The instability growth rate of higher beam density is apparently larger.

We also analyzed the influence of the injected beam energy on the angular magnetic field energy and instability growth rate in Fig. 3(b), where the beam density is fixed at 10^{16} cm^{-3} and the energy varies from 0.4 MeV to 4.0 MeV. High energy beam can certainly cause high magnetic field energy, while the instability growth rate also increases. The development of instabilities of high energy beams is much faster than that of low energy beams.

Sausage instability and kink instability also have an obvious impact on beam energy loss. Fig. 4 shows the spectra of proton beams with densities of 10^{14}, 10^{15}, 5×10^{15}, and 10^{16} cm^{-3} measured by plane II at $t = 13.33$ ns. They have the same initial spectra of 0.4 MeV which are detected by plane I. More details are presented in Table I. When the beam density is 10^{14} cm^{-3}, there is no sausage instability or kink instability and the energy loss is 50 keV in the simulation. According to Bethe's theory [48, 49], the theoretical energy loss of single proton in this condition is 6.02 keV/cm$\times$8 cm = 48.16 keV. When the beam density rises, instabilities show up and the spectrum extends toward lower energy region. Both average energy and minimum energy decrease. As the beam density increases from 10^{14} cm^{-3} to 10^{16} cm^{-3}, the energy loss percentage climbs from 12.5% to 26.0%. Considering the results in Fig. 2, sausage instability and kink instability, especially the latter, make a great influence in the energy loss of beam transport in plasmas.

In summary, the transport for continuous intense proton beams through hydrogen plasmas with density of 10^{18} cm^{-3} and size of 8 cm is simulated by LAPINS PIC code for more than 10 ns. The formation and development of sausage instability and kink instability during the interaction are studied. Simulation and analysis indicate the self-generated magnetic fields, produced by movement of collisional plasmas, take an important role in driving such instabilities. When analysing the instability growth rate and energy loss of injected proton beams, sausage instability and kink instability are found to be significantly determined by the injected beam densities and energies. Our finding might find great applications in inertial confinement fusion research and also might be of interests to the astrophysical community.

This work was supported by Science Challenge Project No. TZ2016005, the National Natural Science Foundation of China (grant numbers 11705141, 11605269, 11775282, U1532263, 11105192, 11075192, 11275241, 11375034, and 11275238), and China Postdoctoral Science Foundation No. 2018M643613.

[1] A. M. de la Ossa, T. J. Mehrling, and J. Osterhoff, Phys. Rev. Lett. **121**, 064803 (2018).

[2] M. Litos, E. Adli, W. An, C. I. Clarke, C. E. Clayton, S. Corde, J. P. Delahaye, R. J. England, A. S. Fisher, J. Frederico, S. Gessner, S. Z. Green, M. J. Hogan, C. Joshi, W. Lu, K. A. Marsh, W. B. Mori, P. Muggli, N. Vafaei-Najafabadi, D. Walz, G. White, Z. Wu, V. Yakimenko, and G. Yocky, Nature **515**, 92 (2014).

[3] N. A. Tahir, F. Burkart, A. Shutov, R. Schmidt, D. Wollmann, and A. R. Piriz, Phys. Rev. E **90**, 063112 (2014).

[4] R. K. Follett, J. A. Delettrez, et al Phys. Rev. Lett. **116**, 155002 (2016).

[5] A. Spitkovsky, Astrophys. J. Lett. **673**, L39 (2008).

[6] C. M. Huntington, F. Fiuza, J. S. Ross, A. B. Zylstra, R. P. Drake, D. H. Froula, G. Gregori, N. L. Kugland, C. C. Kuranz, Nat. Phys. **11**, 173 (2015).

[7] V. N. Zirakashvili, V. S. Ptuskin, and H. J. Voelk, Astrophys. J. **678**, 255 (2008).

[8] A. Spitkovsky, Astrophys. J. Lett. **682**, L5 (2008).

[9] R. Davidson, I. Kaganovich, H. Qin, E. Startsev, D. Welch, D. Rose, and H. Uhm, Phys. Rev. Spec. Top.-Accel. Beams **7**, 114801 (2004).

[10] A. Bret, L. Gremillet, and M. E. Dieckmann, Phys. Plasmas **17**, 120501 (2010).

[11] A. P. L. Robinson, D. J. Strozzi, J. R. Davies, L. Gremillet, J. J. Honrubia, T. Johzaki, R. J. Kingham, M. Sherlock, and A. A. Solodov, Nucl. Fusion **54**, 054003 (2014).

[12] C. Huang, W. Lu, M. Zhou, C. E. Clayton, C. Joshi, W. B. Mori, P. Muggli, S. Deng, E. Oz, T. Katsouleas, M. J. Hogan, I. Blumenfeld, F. J. Decker, R. Ischebeck, R. H. Iverson, N. A. Kirby, and D. Walz, Phys. Rev. Lett. **99**, 255001 (2007).

[13] P. Muggli and the AWAKE Collaboration, Plasma Phys. Control. Fusion **60**, 014046 (2018).

[14] N. Liu, Z. Wang, M. Sun, R. Deiterding, and H. Wang, Aerosp. Sci. Technol. **91**, 456 (2019).

[15] D. Martinez-Ruiz, C. Huete, P. J. Martinez-Ferrer, and D. Mira, J. Fluid Mech. **872**, 889 (2019).

[16] C. K. W. Tam, Annu. Rev. Fluid Mech. **27**, 17 (1995).

[17] A. Brandenburg, A. Nordlund, R. F. Stein, and U. Torkelsson, Astrophys. J. **446**, 741 (1995).

[18] R. Yan, A. V. Maximov, C. Ren, and F. S. Tsung, Phys. Rev. Lett. **103**, 175002 (2009).

[19] D. J. Economou, Plasma Process. Polym. **14**, 1600152 (2017).

[20] S. Markidis, P. Henri, G. Lapenta, K. Ronnmark, M. Hamrin, Z. Meliani, and E. Laure, J. Comput. Phys. **271**, 415 (2014).

[21] H. Fahr, T. Kausch, and H. Scherer, Astron. Astrophys. **357**, 268 (2000).

[22] F. Valentini, P. Travnciek, F. Califano, P. Hellinger, and A. Mangeney, J. Comput. Phys. **225**, 753 (2007).

[23] T. D. Arber, K. Bennett, C. S. Brady, A. Lawrence-Douglas, M. G. Ramsay, N. J. Sircombe, P. Gillies, R. G. Evans, H. Schmitz, A. R. Bell, and C. P. Ridgers, Plasma Phys. Control. Fusion **57**, 113001 (2015).

[24] M. A. Riquelme, E. Quataert, and D. Verscharen, Astrophys. J. **800**, 27 (2015).

[25] J. Kim, B. Qiao, C. McGuffey, M. S. Wei, P. E. Grabowski, and F. N. Beg, Phys. Rev. Lett. **115**, 054801 (2015).

[26] J. Teunissen and U. Ebert, Plasma Sources Sci. Technol. **25**, 044005 (2016).

[27] M. A. Riquelme, E. Quataert, and D. Verscharen, Astrophys. J. **824**, 123 (2016).

[28] L. Collins, I. Kwon, J. Kress, N. Troullier, and D. Lynch, Phys. Rev. E **52**, 6202 (1995).

[29] C. Abrams and D. Graves, J. Appl. Phys. **86**, 5938 (1999).

[30] P. E. Grabowski, M. P. Surh, D. F. Richards, F. R. Graziani, and M. S. Murillo, Phys. Rev. Lett. **111**, 215002 (2013).

[31] K. Yamamoto, Y. Mizuno, S. Hibino, H. Inuzuka, Y. Cao, Y. Liu, and K. Yazawa, Phys. Plasmas **13**, 012106 (2006).

[32] C. E. Torres, H. Parishani, O. Ayala, L. F. Rossi, and L. P. Wang, J. Comput. Phys. **245**, 235 (2013).

[33] G. L. Bryan, M. L. Norman, B. W. O'Shea, T. Abel, J. H. Wise, M. J. Turk, D. R. Reynolds, D. C. Collins, P. Wang, S. W. Skillman, B. Smith, R. P. Harkness, J. Bordner, J.-h. Kim, M. Kuhlen, H. Xu, N. Goldbaum, C. Hummels, A. G. Kritsuk, E. Tasker, S. Skory, C. M. Simpson, O. Hahn, J. S. Oishi, G. C. So, F. Zhao, R. Cen, Y. Li, and the Enzo Collaboration, Astrophys. J. Suppl. Ser. **211**, 19 (2014).

[34] G. Rein, Math. Meth. Appl. Sci. **17**, 1129 (1994).

[35] G. Joyce, G. Knorr, and H. K. Meier, J. Comput. Phys. **8**, 53 (1971).

[36] E. M. Epperlein, G. J. Rickard, and A. R. Bell, Comput. Phys. Commun. **52**, 7 (1988).

[37] K. I. Nishikawa, J. Niemiec, M. Medvedev, B. Zhang, P. Hardee, A. Nordlund, J. Frederiksen, Y. Mizuno, H. Sol, M. Pohl, D. H. Hartmann, M. Oka, and G. J. Fishman, Adv. Space Res. **47**, 1434 (2011).

[38] L. Sironi and A. Spitkovsky, Astrophys. J. Lett. **707**, L92 (2009).

[39] C. B. Schroeder, C. Benedetti, E. Esarey, F. J. Gruener, and W. P. Leemans, Phys. Rev. E **86**, 026402 (2012).

[40] M. Roth, T. Cowan, M. Key, S. Hatchett, C. Brown, W. Fountain, J. Johnson, D. Pennington, R. Snavely, S. Wilks, K. Yasuike, H. Ruhl, F. Pegoraro, S. Bulanov, E. Campbell, M. Perry, and H. Powell, Phys. Rev. Lett. **86**, 436 (2001).

[41] D. Wu, W. Yu, Y. T. Zhao, D. H. H. Hoffmann, S. Fritzsche, and X. T. He, Phys. Rev. E **100**, 013208 (2019).

[42] D. Wu, X. T. He, W. Yu, and S. Fritzsche, Phys. Rev. E **95**, 023207 (2017).

[43] D. Wu, X. T. He, W. Yu, and S. Fritzsche, Phys. Rev. E **95**, 023208 (2017).

[44] D. Wu, X. T. He, W. Yu, and S. Fritzsche, High Power Laser Sci. Eng. **6**, e50 (2018).

[45] D. Wu, W. Yu, S. Fritzsche, and X. T. He, Phys. Rev. E **100**, 013207 (2019).

[46] D. Ryutov, R. Drake, J. Kane, E. Liang, B. Remington, and W. Wood-Vasey, Astrophys. J. **518**, 821 (1999).

[47] A. Bers, *Handbook of plasma physics. Vol.1. Basic plasma physics*, edited by A. Galeev and R. Sudan (North-Holland, 1983).

[48] H. Bethe, Ann. Phys.-Berlin **5**, 325 (1930).

[49] H. Bethe, Z. Phys. **76**, 293 (1932).